Direct pulmonary delivery of solubilized curcumin reduces severity of lethal pneumonia

Boya Zhang,*[,1] Samantha Swamy,*[,1] Sanjay Balijepalli,* Sreehari Panicker,* Jashitha Mooliyil,* Matthew A. Sherman,† Jaakko Parkkinen,‡ Krishnan Raghavendran,* and Madathilparambil V. Suresh*[,2]

*Department of Surgery, University of Michigan, Ann Arbor, Michigan, USA; †Department of Pediatrics, Children's National Medical Center, Washington, DC, USA; and ‡Institute of Biomedicine, University of Helsinki, Helsinki, Finland

ABSTRACT: Acute respiratory distress syndrome (ARDS), the most severe form of acute lung injury, is associated with reduced lung compliance and hypoxemia. Curcumin exhibits potent anti-inflammatory properties but has poor solubility and rapid plasma clearance. To overcome these physiochemical limitations and uncover the full therapeutic potential of curcumin in lung inflammation, in this study we utilized a novel water-soluble curcumin formulation (CDC) and delivered it directly into the lungs of C57BL/6 mice inoculated with a lethal dose of *Klebsiella pneumoniae* (*KP*). Administration of CDC led to a significant reduction in mortality, in bacterial presence within blood and lungs, as well as in lung injury, inflammation, and oxidative stress. The expression of *Klebsiella* hemolysin gene; TNF-α; IFN-β; nucleotide-binding domain, leucine-rich–containing family, pyrin domain–containing-3; hypoxia-inducible factor 1/2α; and NF-κB were also decreased following CDC treatment, suggesting modulation of the inflammasome complex and hypoxia signaling pathways as an underlying mechanism by which CDC reduces the severity of pneumonia. On a cellular level, CDC led to diminished cell death, improved viability, and protection of human lung epithelial cells *in vitro*. Overall, our studies demonstrate that CDC administration improves cell survival and reduces injury, inflammation, and mortality in a murine model of lethal gram-negative pneumonia. CDC, therefore, has promising anti-inflammatory potential in pneumonia and likely other inflammatory lung diseases, demonstrating the importance of optimizing the physicochemical properties of active natural products to optimize their clinical application.—Zhang, B., Swamy, S., Balijepalli, S., Panicker, S., Mooliyil, J., Sherman, M. A., Parkkinen, J., Raghavendran, K., Suresh, M. V. Direct pulmonary delivery of solubilized curcumin reduces severity of lethal pneumonia. FASEB J. 33, 13294–13309 (2019). www.fasebj.org

KEY WORDS: phagocytosis · macrophages · apoptosis · capillary Western blot · MTT

Acute respiratory distress syndrome (ARDS) is a life-threatening, overexuberant inflammatory response caused by a variety of insults (1). The severity of ARDS is associated with poor prognosis and higher mortality (2, 3). Several factors increase the risk of ARDS, including sepsis, acid aspiration, major trauma, lung contusion (LC), acute pancreatitis, massive transfusions, and bacterial pneumonia (4–8). Bacterial pneumonia remains a significant cause of morbidity and mortality in modern intensive care units (9). The incidence of ventilator-associated pneumonia steadily increases despite the introduction of ventilator-associated pneumonia bundles in the care of critically ill patients (10, 11). Infection (12), such as sepsis and pneumonia, precipitates ARDS in more than half of all reported cases. *Klebsiella pneumoniae* (*KP*) (13) are common gram-negative bacteria that is frequently implicated in ARDS (14).

Curcumin is a polyphenol extracted from turmeric, which belongs to the *Zingiberaceae* family. It has been shown that curcumin has a broad range of beneficial properties both *in vitro* and *in vivo*, including anti-inflammatory, antitumor, antioxidant, and antimicrobial effects (15–17). Recent studies have demonstrated that curcumin reduces inflammation, improves morbidity, and decreases mortality in models of inflammatory disease such as rheumatoid arthritis and inflammatory bowel disease as well as common malignancies including colon,

ABBREVIATIONS: AEC, alveolar epithelial cell; ALI, acute lung injury; AM, alveolar macrophage; ARDS, acute respiratory distress syndrome; ASC, apoptosis-associated speck-like protein containing caspase activation and recruitment domain (CARD); BAL, bronchoalveolar lavage fluid; CD, cyclodextrin; CDC, water-soluble curcumin formulation; CFU, colony forming unit; Fc, flow cytometry; FER, feline sarcoma–related kinase; FIZZ-1, retnla resistin9like α; HIF, hypoxia-inducible factor; KC, keratinocyte chemoattractant; *Khe*, *Klebsiella* hemolysin gene; LC, lung contusion; M1, macrophage phenotype 1; M2, macrophage phenotype 2; MIP-2, macrophage inflammatory protein 2; MPO, myeloperoxidase; MTT, tetrazolium dye reduction assay; NLRP-3, nucleotide-binding domain, leucine-rich-containing family, pyrin domain-containing-3; PV, pressure volume; qRT-PCR, quantitative RT-PCR

[1] These authors contributed equally to this work.

[2] Correspondence: Department of Surgery, University of Michigan, 1150 West Medical Center Drive, Ann Arbor, MI 48109, USA. E-mail: madathil@umich.edu

doi: 10.1096/fj.201901047RR

This article includes supplemental data. Please visit *http://www.fasebj.org* to obtain this information.

0892-6638/19/0033-13294 © FASEB

stomach, heart, lung, breast, and skin cancers (18–22). However, the poor solubility and chemical instability of curcumin under physiologic conditions limit its bioavailability and clinical efficacy (23).

We previously developed a stable, water-soluble curcumin formulation (CDC) in which the compound is complexed with hydroxyalkyl-substituted γ-cyclodextrin (CD) (24, 25). CDs were previously tested in nebulized inhaled drug formulations, with some reports indicating that CD enhances pulmonary penetration. The CDC was administered intravenously to beagles at doses as high as 10 mg/kg twice daily for 14 d, without observed adverse effects (24). After repeated daily administration, tetrahydocurcumin sulfate, the major metabolite, peaked at 30 min and mostly cleared the system by 60 min. The rapid plasma clearance of curcumin after systemic CDC administration supports our choice of pulmonary administration for further *in vivo* studies.

We have previously shown that direct delivery of the CDC to the lung following exposure to LPS reduces the severity of acute lung injury (ALI) in mice (24). Here, we investigated the role of CDC in a clinically relevant model of gram-negative pneumonia in both male and female mice. We demonstrate for what we believe to be the first time the ability of a curcumin formulation to effectively reduce inflammation and mortality in a lethal model of gram-negative pneumonia, thus encouraging the development of novel natural product–based therapeutics for bacterial pneumonia and ARDS.

MATERIALS AND METHODS

Animals

Male and female age-matched (8–10 wk) C57BL/6 (The Jackson Laboratory, Bar Harbor, ME, USA) mice were used in this study. All procedures performed were approved by the Institutional Animal Care and Use Committee at the University of Michigan and complied with state, federal, and National Institutes of Health (NIH, Bethesda, MD, USA) regulations.

Curcumin preparation

Curcumin was prepared as previously described. Briefly, hydroxypropyl-γ-CD was dissolved to a concentration of 112 g/L in 0.18 M sodium hydroxide solution. Curcumin (Curcumin C3 Complex; Sabinsa Corp., East Windsor, NJ, USA) was added to a concentration of 15 g/L. The solution was agitated, and after complete dissolution of curcumin, the pH was adjusted to 6.0 with a mixture of acids. The solution was filtered and filled aseptically into sterile vials that were then capped and sealed. The recovered CDC solution contained 12 g/L curcumin and 93 g/L CD in 20 mM sodium citrate in a total of 100 mM NaCl solution. Endotoxin content was <1.8 IU/ml as measured by the Limulus amoebocyte lysate gel clot method. The CDC solution was stored at 2–8°C and protected from light. The CD vehicle was prepared in the same way but without the addition of curcumin (24, 25).

Bacterial pneumonia model

KP, strain 43816, serotype 2 was purchased from American Type Culture Collection (ATCC; Manassas, VA, USA). This microbial strain was cultured overnight in trypticase soy broth (Becton Dickinson, San Diego, CA, USA) with reinoculation the following morning into fresh medium to bring the bacteria into log-growth phase. The bacteria were centrifuged at 600 *g* and 4°C for 10 min, washed with sterile 0.9% normal saline, centrifuged again, and then resuspended in sterile saline. Optical density was read on a spectrophotometer (Milton Roy, Rochester, NY, USA) at a wavelength of 600 nm. Appropriate serial dilutions were subsequently performed to achieve a concentration of 500 colony forming units (CFUs) of bacteria per 30 μl of inoculum. Mice were inoculated with the bacterial suspension or vehicle *via* deep oral hypopharyngeal injection under isoflurane anesthesia (26). Lastly, the CDC was administered 2 h before as well as 2, 6, and 24 h after injection with KP. The CDC concentration was 30 μg/30 μl per mouse (CDC frequency was chosen based on our previous study). Animals were allowed to recover spontaneously. Survival was monitored for 10 d, and animal health and survival data were recorded every 8 h. The survival study was repeated twice, with CDC administered before and after *KP*.

Determination of bacterial survival in the lungs and blood

Bacterial loads in the lungs and blood of *KP* and CDC mice were determined at 24 and 48 h. Lungs were removed and maintained in sterile conditions. Both lungs were homogenized in 1 ml of ice-cold PBS. A small aliquot (100 μl) of tissue homogenate was serially diluted in sterilized PBS, plated on 5% sheep blood agar, and incubated overnight at 37°C, after which the number of colonies was determined. For blood CFU determination, blood was collected *via* cardiac puncture using a sterile 18-gauge needle. To measure bacteremia, 100 μl of undiluted blood was plated onto 5% sheep blood agar plates (Thermo Fisher Scientific, Waltham, MA, USA) and incubated at 37°C for 24 h, after which colonies were counted. If no colonies were present, culture plates were kept for an additional 48 h in the incubator to confirm no growth of delayed organisms (27–29).

Lung pressure-volume mechanics

Immediately following exsanguination, pulmonary respiratory mechanics were measured after blood samples were obtained. Mice were further exsanguinated by transection of the abdominal inferior vena cava. An 18-gauge metallic cannula was inserted into the trachea through a midline cervical exposure. Animals were then connected to a Scireq flexiVent (Scireq, Montreal, QC, Canada) that allows for simultaneous ventilation and data capture. Immediate postmortem ventilation was performed with the following parameters: tidal volume 10 ml/kg, respiratory rate 150 breaths per minute, and positive-end expiratory pressure 2 cmH_2O. With the pressure-volume (PV) ramp volume regulated, controlled inflation and deflation was performed to measure quasi-static compliance values (30).

Albumin concentrations in bronchoalveolar lavage

Albumin concentrations in bronchoalveolar lavage fluid (BAL) were measured by ELISA using polyclonal rabbit anti-mouse albumin antibodies and horseradish peroxidase–labeled goat anti-rabbit IgG (Bethyl Laboratories, Montgomery, TX, USA) (31, 32).

Determination of cytokine levels in BAL and lungs

Soluble concentrations of IL-1β, IL-4, IL-6, IL-10, IL-13, IL-17, IL-22, macrophage inflammatory protein 2 (MIP-2), chemokine

ligand 6 (CCL6) (monocyte chemoattractant protein 1), CCL12 (monocyte chemotactic protein 5), receptor for advanced glycation end products, myeloperoxidase (MPO), IFN-γ, TNF-α, and keratinocyte chemoattractant (KC) in the BAL and lungs following pneumonia and CDC administration were determined using ELISA. Antibody pairs (1 capture antibody and 1 biotinylated-reporter antibody) and recombinant cytokines for these assays were obtained from R&D Systems (Minneapolis, MN, USA) (5).

Cytospin cell count

BAL cells were centrifuged at 600 *g* for 5 min using a Cytospin II (Thermo Fisher Scientific), stained with Diff-Quik (Dade Behring, Deerfield, IL, USA), and analyzed by examination under a light microscope at ×20 magnification as previously described in refs. 30 and 33.

Tetrazolium dye reduction assay of bacterial killing

The bacterial killing capacity of alveolar macrophages (AMs) was quantified using tetrazolium dye reduction assay (MTT) (34). Wild-type mice were administered CDC, *KP*, or *KP* + CDC. AMs were collected and seeded into (triplicate) 96-well plates, 1 experimental (37°C) plate, and 1 control (4°C). Cells from both plates were infected with *KP* (2.3×10^8 CFU/ml; the multiplicity of infection 50:1) for 30 min at 37°C. Cells on the experimental plate were washed and then incubated at 37°C for 90 min, whereas cells on the control plate were washed and then lysed with 0.5% saponin in tryptic soy broth (MilliporeSigma, Burlington, MA, USA) and placed at 4°C. After 90 min, cells from the experimental plate were lysed with 0.5% saponin in tryptic soy broth. Both plates were then incubated at 37°C for 2.5 h. A total of 5 mg/ml MTT (MilliporeSigma) was added to each plate and incubated for 30 min, and the absorbance at 595 nm (A_{595}) was read. Results were expressed as a percentage of survival of ingested bacteria normalized to the percentage of control, where the A_{595} experiment values were divided by the average of the A_{595} control values using the following formula: survival of ingested bacteria = (A_{595} experimental plate/A_{595} control plate) × 100%.

In vitro phagocytosis assay

Phagocytosis assays were performed as previously described by Takala *et al.* (12). Briefly, AM was isolated from BAL after administration of *KP* and CDC, plated onto a 2×10^5 cells/well plate, and cultured overnight in DMEM medium. Wells were aspirated and replaced with 50 μl serum-free medium. AM was then incubated with FITC-labeled, heat-killed *KP*. Phagocytosis of FITC-labeled bacteria was measured after quenching of non-ingested bacteria with trypan blue (32, 33).

Ex vivo phagocytosis following *KP* by mouse macrophages

Phagocytosis assays were performed with adherent macrophages as previously described by Suresh *et al.* (30) but with modifications. *KP* was opsonized in fresh 5% normal fetal bovine serum for 30 min at 37°C, washed in PBS, and resuspended in Roswell Park Memorial Institute (RPMI) 1640 /H medium at 1000 CFUs. Macrophages were added (3×10^5) to serum-coated chambered 8-well tissue culture plates and allowed to adhere at room temperature for 1 h. Cells were washed with PBS, non-adherent cells were removed, and the remaining macrophages were combined with 10^3 *KP*. The assay chamber was incubated for 1 h at 37°C to initiate phagocytosis. Macrophages were then washed with cold PBS. Cells were fixed with 4% paraformaldehyde for 10 min on ice, followed by 10 min at room temperature. The fixative was removed by aspiration, and then the samples were washed 3 times with PBS and incubated in blocking buffer (5% goat serum in PBS) for 30 min at room temperature. To detect ingested bacteria, macrophages were permeabilized with 0.3% Triton X-100 for 10 min at room temperature prior to incubation with FITC-labeled *Klebsiella* pAb (Thermo Fisher Scientific) for 1 h at room temperature. Nuclei were stained with DAPI. Cells on coverslips were then mounted in mounting media (Agilent Technologies, Santa Clara, CA, USA), and photomicrographs of the invasive sections were analyzed digitally using Photoshop software v.9.0.2 (Adobe, San Jose, CA, USA).

Flow-cytometry, apoptosis-annexin V-FITC staining

Apoptosis analysis was performed as previously described. Briefly, cells were labeled with Annexin V (BioLegend, San Diego, CA, USA) and incubated for 20 min at room temperature. After washing with Annexin V binding buffer, cells were incubated for 10 min with Live/Dead stain (Thermo Fisher Scientific). Cells were washed and blocked with flow cytometry (Fc) block (CD16/32) and then stained with the following fluorochrome-conjugated mouse antibodies: Ly6C-FITC, Gr-1-PE, CD11c-APCCy7, F4/80-AF488, and CD11b-PE-Cy7 (BioLegend, BD Biosciences, San Jose, CA, USA). Data were analyzed using FlowJo software (Treestar, Ashland, OR, USA) (30, 31).

TaqMan quantitative PCR

Total RNA was prepared from whole lung lysate and reverse transcribed into cDNA using Moloney Murine Leukemia Virus Reverse Transcriptase (M-MLV RT; Thermo Fisher Scientific). cDNA was then amplified by real-time quantitative TaqMan PCR using an ABI Prism 7700 sequence detection system (GraphPad, La Jolla, USA). Glyceraldehyde 3-phosphate dehydrogenase was analyzed as an internal control. TaqMan gene expression reagents or SYBR Green Master PCR Mix (Thermo Fisher Scientific) were used to detect genes responsible for inflammation. Data were expressed as the fold-change in transcript expression. Fold difference in mRNA expression between treatment groups was determined by software developed by Thermo Fisher Scientific (30, 31).

Western blot

Mouse lungs were lysed in ice-cold lysis buffer, mixed with a commercial sample buffer (Thermo Fisher Scientific), and heated at 95°C for 5 min. Samples were then electrophoresed on SDS-polyacrylamide gels after which the gels were transferred to PVDF membranes. Blots were incubated overnight at 4°C with various primary antibodies and followed by appropriate secondary antibody. They were then washed, and the signal was detected using a Super Signal chemiluminescent substrate Western blotting reagent (Pierce Biotechnology, Waltham, MA, USA) with chemiluminescent-sensitive film (31).

Histology

Lung sections were fixed in formalin, embedded in paraffin, sectioned, and stained with hematoxylin and eosin. Histologic findings such as peribronchial, parenchymal, and perivascular

cell infiltration were semiquantitatively graded in a blinded manner (24, 33).

Cell culture

Human lung epithelial cells (A549) (ATCC) were grown as a monolayer in 5% CO2 at 37°C in FK12 medium supplemented with 10% heat-inactivated fetal bovine serum, 50 U/ml penicillin, and 50 mg/ml streptomycin. Cells were plated in 6-well culture plates or 8-well chambered plates for various experiments.

Curcumin administration *in vitro*

Human lung epithelial cells (A549) were plated at densities of 4×10^5 cells/well in 6-well plates. After 24 h of incubation, the medium was changed to serum-free DMEM followed by 24-h culture. Cells were then treated with or without curcumin (200 μM concentrations of CDC) for 2 h at 37°C in 5% CO_2. After incubation with CDC, the medium was discarded, and cells were added to a new antibiotic-free medium and treated with *KP* (100 CFUs). Cells were then cultured for an additional 24 h after which samples were collected (24).

NF-κB immunocytochemistry

Human lung epithelial cells (A549) were seeded in 8 chambered glass plates. After 24 h of incubation, cells were treated with *KP* in the presence and absence of CDC for 24 h at 37°C in 5% CO_2. Control cells were exposed to *KP* and CDC alone. After incubation, the medium was changed, and cells were washed 3 times with PBS. Cells were fixed by adding formaldehyde directly, for 15 min at room temperature. Next, cells were washed with PBS, permeabilized with 0.2% Triton X-100 (MilliporeSigma), washed 2 more times with PBS, and blocked with PBS containing 1% bovine serum albumin. This was followed by incubation in NF-κBp65 (Cell Signaling Technology, Danvers, MA, USA) followed by incubation in Alexa fluorescent-labeled secondary antibodies (Thermo Fisher Scientific) for 1 h. Nuclei were stained with DAPI. Cells were then mounted on coverslips in mounting media (Agilent), and photomicrographs of the invasive sections were analyzed digitally using Photoshop software v.9.0.2.

Capillary Western immunoassay

Western immunoassay analysis was performed with a Western immunoassay system (004–600; Protein Simple, San Jose, CA, USA) according to the manufacturer's instructions using a 12–230 kDa separation module (SM-W004; Protein Simple) and an anti-mouse detection module (DM-002; Protein Simple) (35). Briefly, protein samples were diluted 10-fold in sample buffer (100-fold diluted 10× Sample Buffer 2 from the Separation Module), then mixed with Fluorescent Master Mix (ProteinSimple, Centennial, CO, USA) and heated at 95°C for 5 min. The samples, blocking reagent (antibody diluent), primary antibodies (in antibody diluent), horseradish peroxidase–conjugated secondary antibodies, and chemiluminescent substrate were pipetted onto the plate of the separation module.

Statistical methods

Data were expressed as means ± SEM. Statistical significance was estimated using 1-way ANOVA (GraphPad Prism 7.01). Individual intergroup comparisons were analyzed using a 2-tailed, unpaired Student's *t* test with Welch's correction. Survival curves (Kaplan-Meier plot) were compared using log-rank tests (26). Fluorescence recovery analysis was performed using ImageJ (NIH) (36). Values of $P < 0.05$ were considered significant (30, 31).

RESULTS

Survival is enhanced and the bacterial burden is reduced by CDC administration

Here, we examined the protective effect of CDC in a murine model of pneumonia using *KP*. In the first set of experiments, the CDC was administered 2 h before inoculation with *KP*. Survival was monitored for 10 d. All *KP* mice died within 5 d. However, survival rates were significantly improved (60%) in mice that received CDC. Mice unexposed to *KP* had 100% survival (**Fig. 1*A***). Survival experiments were repeated twice ($n = 10$/group, a total of 40 animals). Next, the CDC was administered 2 h after inoculation with *KP* and survival was monitored for 10 d. Again, the CDC administration led to 60% survival. All mice exposed to *KP* that did not receive CDC died within 5 d. This survival experiment was repeated twice ($n = 10$/group, a total of 40 animals) (Fig. 1*B*). In another set of experiments, the CDC was administered 6 and 24 h after *KP* administration and survival was monitored for 10 d. The survival rates were significantly better in mice that received CDC 6 h after pneumonia. In contrast, only 20% of mice that received CDC 24 h after pneumonia survived at 10 d, but mortality was still significantly decreased compared to mice that did not receive CDC ($n = 10$/group, total 30 animals) (Fig. 1*C*) (*$P < 0.05$ by log-rank test). For all further experiments, CDC was administered 2 h after bacterial inoculation to correspond to the initiation of pneumonia treatment more closely.

Next, bacterial counts in the lungs and blood were assessed. There were significantly reduced bacterial counts in the lungs of mice that received CDC compared to *KP* alone ($n = 4$/group) (Fig. 1*D*). Mice that were administered CDC exhibited significantly reduced bacterial burden both in terms of growth on blood agar and CFUs at 24 and 48 h compared to *KP* alone ($n = 4$ per group). There was no growth in the vehicle and CDC groups alone (Fig. 1*E*, *F*). Taken together, the data suggest that the CDC improves bacterial clearance and survival in mice inoculated with *KP* in a lethal model of gram-negative pneumonia.

Permeability injury and inflammation are modulated by CDC administration

We have previously demonstrated that curcumin is extensively taken up by cells in the lung following CDC administration (24). We next examined the total number of cells in the BAL following inoculation with *KP* and CDC administration. Fc revealed significantly more cells in mice exposed to *KP* compared to vehicle and controls, but there was no significant difference between the 2 pneumonia groups (**Fig. 2*A***). Similarly, the level of monocytes at 24 h was higher in mice exposed to *KP* compared to vehicle and

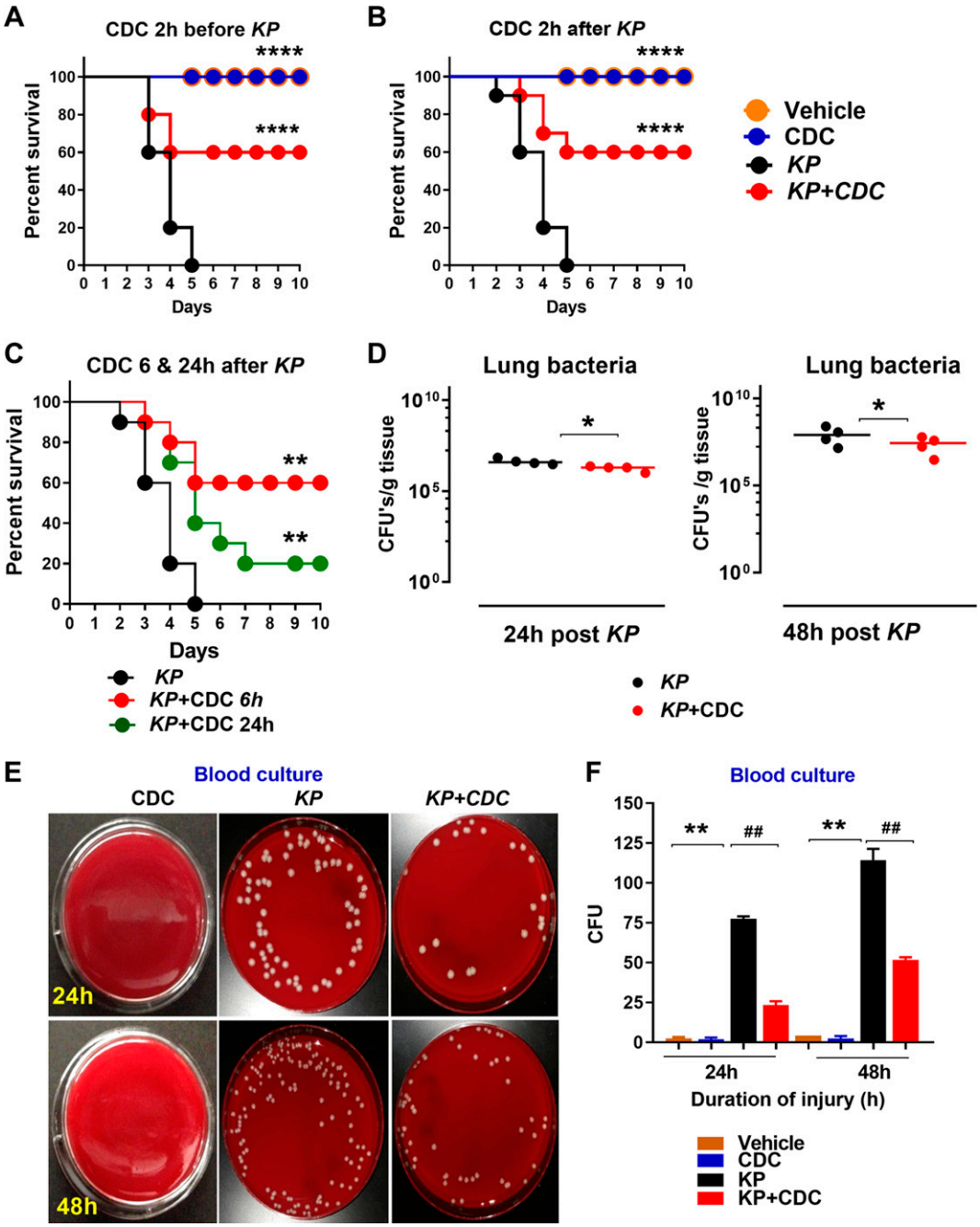

Figure 1. CDC administration enhances survival and reduces bacterial burden in blood and lungs following *KP*. *A*, *B*) Survival studies: wild-type mice ($n = 10$ mice/group) were infected with 500 CFUs of *KP*. CDC was administered 2 h before (*A*) and after (*B*) *KP*. Survival was monitored over 10 d. In the third study, CDC was administered 6 and 24 h after *KP*. *C*) Survival was determined 10 d ($n = 10$ mice/group). Significance values were determined with the log-rank Mantel-Cox test. $^{**}P < 0.05$ *KP vs.* CDC; $^{*}P < 0.05$ *KP vs.* *KP* + CDC. *D–F*) Bacterial burden in the lung (*D*) and blood (*E*, *F*) was assessed 24 and 48 h following inoculation ($n = 4$/group). $^{*}P < 0.5$ CDC *vs.* *KP*, $^{\#}P < 0.5$ *KP vs.* *KP* + CDC.

controls, but there was no significant difference between the 2 pneumonia groups (Fig. 2*B*). Additionally, there was no significant difference in macrophage recruitment (Fc and cytospin) between *KP* and *KP* + CDC mice at both the 24- and 48-h intervals (Fig. 2*C*, *D*). We next assessed the apoptotic response in *KP* mice with and without CDC. First, we examined the level of macrophages by macrophage phenotype 1 (M1) and macrophage phenotype 2 (M2). In *KP* mice, the M1 was higher compared to mice that treated with CDC (Fig. 2*E*). M2s, however, were found to predominate in *KP* mice that received CDC compared to *KP* alone (Fig. 2*F*). Moreover, M1 and M2 apoptosis were lower in *KP* + CDC mice compared to *KP* alone (Fig. 2*G*, *H*). These data suggest that CDC treatment better preserves macrophages against apoptosis. Finally, the level of neutrophils was significantly higher (Fc and cytospin evaluation) at 24 h in the pneumonia group that received CDC compared to *KP* alone (Fig. 2*I*, *J*).

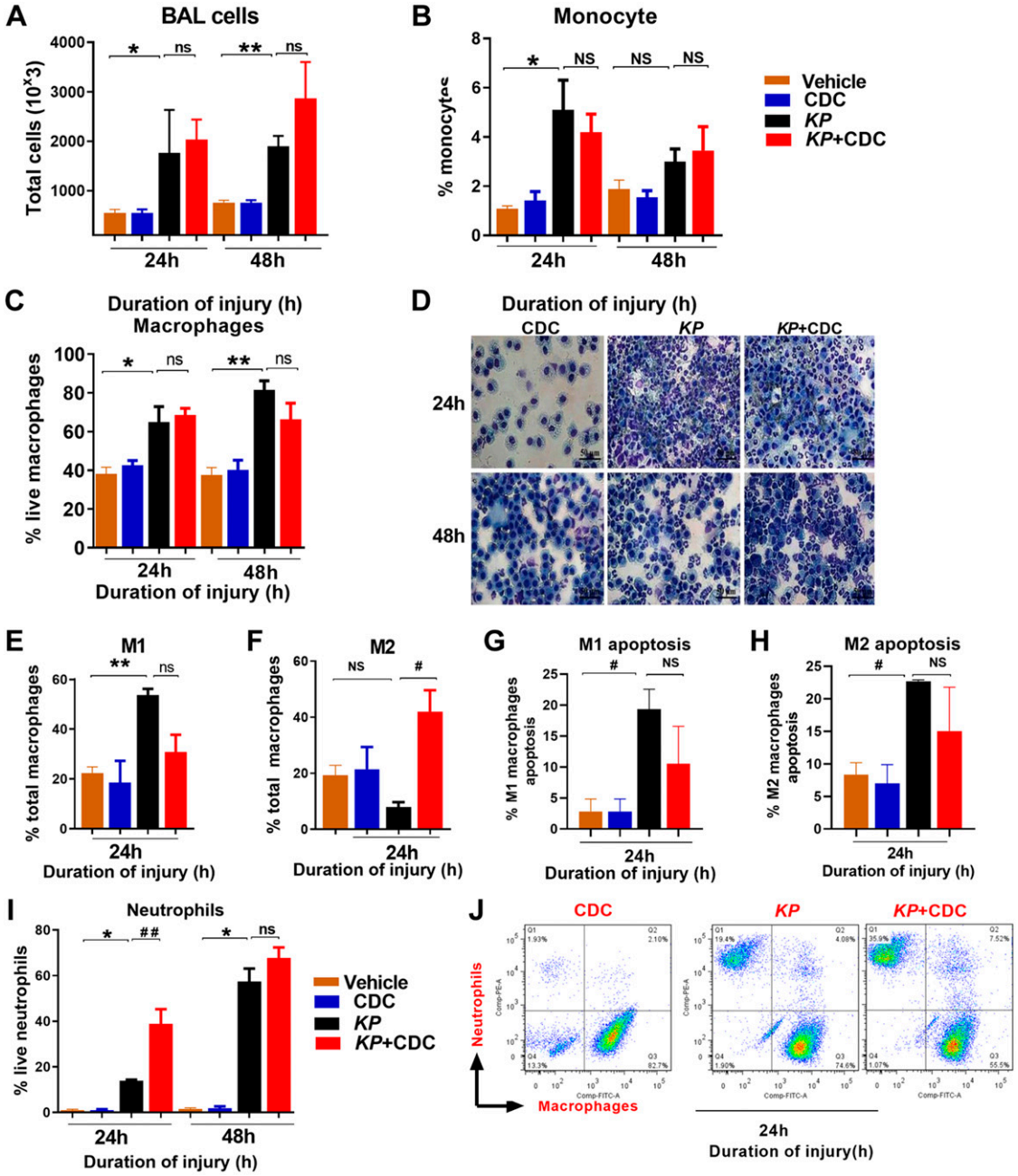

Figure 2. *A*, *B*) CDC administration attenuates injury and inflammation following pneumonia. BAL cells: Fc data demonstrate the total number of cells (*A*) and the total number of monocytes (*B*) following *KP* and CDC administration. *C*, *D*) Representative Fc (*C*) and cytospin (*D*) data show the total number of macrophages following *KP* and CDC administration ($n = 6$/group). *E*, *F*) Fc data show the total number of M1s (*E*) and M2s (*F*) following KP and CDC administration ($n = 6$/group). *G*, *H*) M1s (*G*) and M2s (*H*) apoptosis were measured by Fc. *I*, *J*) The Fc and cytospin data reveal the level of neutrophils (*I*, *J*) the *KP* + CDC group compared to *KP* alone at both time points ($n = 6$/group). Samples were analyzed using a 2-tailed, unpaired Student's *t* test with Welch's correction. $^{*}P < 0.05$ CDC *vs.* *KP*, $^{\#}P < 0.05$ *KP vs.* *KP* + CDC.

Lung compliance is better preserved by CDC administration

We have previously shown that the acute inflammatory response in LC and pneumonia is responsible for the deficits in oxygenation, increases in quasi-static pulmonary compliance and severe permeability injury (26, 30, 37). To determine the extent of the mechanical injury, PV measurements were taken at different time intervals following *KP* administration with and without CDC. Pulmonary compliance and total lung capacity at 30 cmH_2O were significantly better in *KP* mice that received CDC than in *KP* mice alone at both time points (**Fig. 3*A*, *B***). These data suggest that CDC treatment protects against worsening mechanical lung function following pneumonia.

We also found that the level of BAL albumin, a marker of permeability injury, was significantly lower in *KP* + CDC mice at both 24 and 48 h (Fig. 3C). Finally, histologic evaluation of hematoxylin and eosin–stained lung sections revealed significantly reduced injury in pneumonia mice

that received CDC compared to *KP* alone at both time points (Fig. 3*D*). Taken together, the above data indicate that delivery of CDC protects against worse permeability injury and overall destruction of lung architecture following gram-negative bacterial pneumonia exposure.

Production of proinflammatory cytokines is diminished by CDC administration

To determine the role of CDC in the production of neutrophil activity, the levels of proinflammatory cytokines (IL-1β, IL-6, TNF-α), KC, MIP-2, and MPO were measured in the BAL and lungs. In the BAL, the levels of IL-1β, IL-6, KC, and MIP-2 were significantly reduced in pneumonia mice that received CDC in conjunction with *KP* compared to *KP* alone (**Fig. 4*A–H***). TNF-α was significantly elevated in *KP* + CDC mice only at 24 h in the BAL but significantly elevated at both time points in the lung (Fig. 4*I*, *J*). MPO is a significant constituent of neutrophil cytoplasmic granules. In the BAL, MPO was significantly reduced at both time points in *KP* + CDC mice compared to *KP* alone (Fig. 4*K*) (significance is not shown on Fig. 4*K* between *KP* and *KP* + CDC groups at the 24-h time point above the bars). There

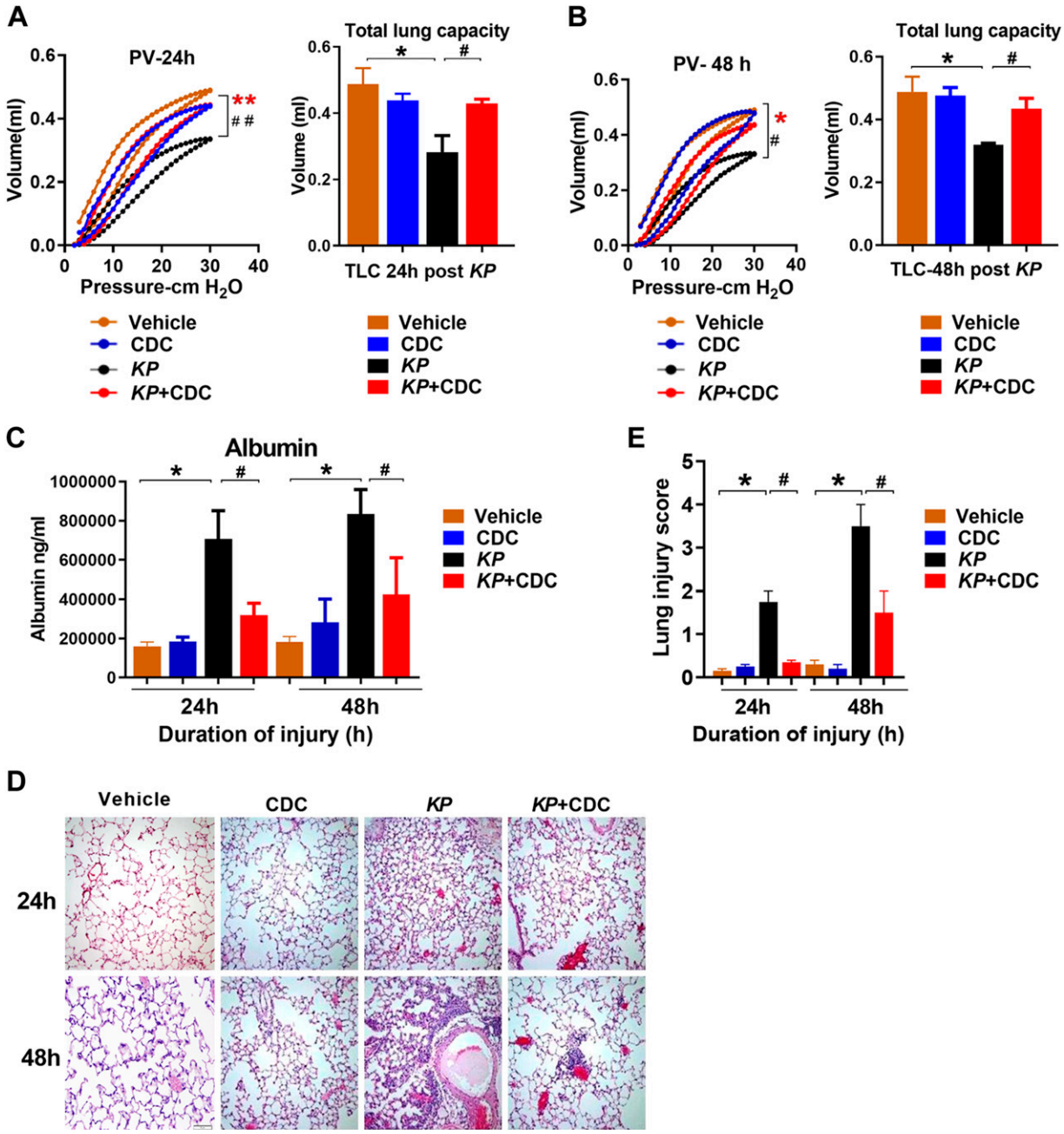

Figure 3. CDC administration attenuates injury following pneumonia. *A*, *B*) PV mechanics: Closed-chest PV mechanics were measured at 24 h (*A*) and 48 h (*B*) after *KP* ($n = 6$/group). *C*) Permeability injury: Albumin concentration in the BAL was determined by ELISA ($n = 16$). *D*, *E*) Pathologic injury: Representative hematoxylin and eosin lung sections at 24 and 48 h following *KP* and CDC administration ($n = 3$/group) are shown at ×400 original magnification (*D*), and the degree of pathologic injury was calculated (*E*). Statistical analysis was performed at each time point with a 2-tailed, unpaired Student's *t* test with Welch's correction. $^{*}P < 0.05$ CDC *vs.* *KP*; $^{\#}P < 0.05$ *KP vs.* *KP* + CDC.

was no significant difference in lung MPO levels at both time points (Fig. 4*L*).

Additionally, monocyte chemoattractant protein 1was significantly decreased at 24 h in the BAL and 48 h in the lungs of *KP* + CDC mice (Supplemental Fig. S1*A, B*). Monocyte chemotactic protein 5 was significantly lower in the BAL of *KP* + CDC mice only at 48 h (Supplemental Fig. S1*C, D*). IL-4 and IL-13 were initially identified as products of activated Th2 cells, and previous studies have shown that they possess a variety of immunomodulatory properties concerning B cells (38, 39). Here, both IL-4 and IL-13 were significantly elevated in *KP* + CDC mice at 24 h in both the BAL and lungs (Supplemental Fig. S1*E, H*). IFN-γ was found to be significantly lower in the lungs of *KP* + CDC at 48 h compared to *KP* alone (Supplemental Fig. S1*I*), but there was no difference in the BAL (unpublished results). Receptor for advanced glycation end products was also elevated in the BAL and lungs of *KP* + CDC mice only at 24 h (Supplemental Fig. S1*J, K*). Finally, there was no difference in the levels of IL-17, IL-22, and IL-10, an important anti-inflammatory cytokine, in the BAL of *KP* and *KP* + CDC mice (unpublished results). Taken together, these data overall demonstrate that CDC down-regulates the acute inflammatory response following pneumonia.

AM phagocytosis is improved following CDC administration

AMs (33, 40) are the predominant immune cells in the lungs during initial infection, and increased susceptibility to bacterial infection is associated with defects in AM phagocytosis. Here, we examined AM phagocytosis *ex vivo* following inoculation with *KP*. Cells were harvested 24 h following *KP* administration in the presence and absence of CDC and later subjected to immunofluorescence staining with *KP* (green) and nuclear staining with DAPI. The most intense phagocytosis was found in AM taken from *KP* + CDC mice (**Fig. 5*A***). AM was also harvested from the BAL to measure the rate of phagocytosis by opsonized and non-opsonized relative phagocytic activity *in vitro*. Both opsonized and non-opsonized phagocytosis was significantly higher in *KP* + CDC mice at 24 h compared to *KP* alone (Fig. 5*B, C*). Poor bacterial clearance is associated with increased susceptibility to infection, and increased phagocytosis is a critical component of the immune response to bacterial pneumonia. Next, AM intracellular clearance of *KP* in the absence and presence of CDC was assessed using the MTT assay. Intracellular bacterial clearance by AM was significantly higher in *KP* + CDC mice compared to *KP* alone, as indicated by the significantly lower number of surviving bacteria (Fig. 5*D*).

Finally, the expression of the lung *Klebsiella* hemolysin gene (*Khe*), a species-specific gene for *KP*, was significantly decreased at both 24 and 48 h in *KP* + CDC mice compared to *KP* alone (Fig. 5*E*). As a whole, these data suggest that CDC leads to improved AM phagocytosis and clearance, protecting against *KP*. Statistical analysis was performed with 2-tailed, unpaired *t* test with Welch's.

RNA transcription of proinflammatory genes is attenuated by CDC administration

We have previously found that proinflammatory and hypoxia-related genes drive the acute inflammatory response following LC and acid-induced aspiration (31, 37). Here, RNA was isolated from the lungs of CDC, *KP*, and *KP* + CDC mice and the expression of specific proinflammatory genes including NOS-2, arginase-1, and retnla resistin-like α (FIZZ-1) were measured by quantitative RT-PCR (qRT-PCR). Unconditional expression of the M1 (NOS-2) indicates significant injury and is associated with increased production of proinflammatory cytokines. Furthermore, high expression of the M2 is characterized by increased up-regulation of the FIZZ-1/arginase pathway. The expression of NOS-2 was significantly lower in pneumonia mice that received CDC (**Fig. 6*A***). While the expression of arginase-1 was significantly higher in *KP* + CDC compared to *KP* mice at both time points, the expression of FIZZ-1 was only significantly higher at 48 h (Fig. 6*B, C*). CDC, therefore, induced mice exposed to *KP* to exhibit the protective M2 AM phenotype, as evidenced by decreased expression of NOS-2 and increased expression of both arginase-1 and FIZZ-1.

We have also recently reported that activation of hypoxia-inducible factor (HIF)-1α is crucial for the development of acute inflammation and injury following LC and aspiration-induced lung injury (5, 37). In the present study, the expression of HIF-1α and HIF-2α was measured following *KP*. Expression of HIF-1α at both time points and HIF-2α at 24 h was significantly elevated in *KP* mice compared to *KP* + CDC mice, in which the expression was maintained close to control levels (Fig. 6*D, E*). It is therefore likely that CDC reduces inflammation in part through regulation of early hypoxic signaling pathways.

The expression of other proinflammatory genes, including IFN-β, TLR-2, and TLR-4, were also measured. The expression of IFN-β was significantly elevated at 48 h in *KP* mice (Supplemental Fig. S2*A*). In *KP* mice, the expression of TLR-2 was significantly elevated at 24 h, and the expression of TLR-4 was significantly elevated at both time points compared to mice that received CDC (Supplemental Fig. S2*B, C*). We have also recently found that feline sarcoma–related kinase (FER), a tyrosine-protein kinase gene, is involved in the recruitment and activation of inflammatory monocytes and macrophages as well as in modifications of known signaling transduction pathways that enhance bacterial clearance and improve survival (26, 27). Here, the levels of FER were significantly higher in *KP* + CDC mice compared to *KP* mice at 48 h, both CDC and *KP* + CDC mice at 48 h (Supplemental Fig. S2*F*).

Systemic inflammation and inflammasome activation are attenuated by CDC administration

To examine the effect of CDC on serum systemic inflammation, the expression of proinflammatory cytokines, including IL-1β, IL-6, and TNF-α, were measured at 24 h in

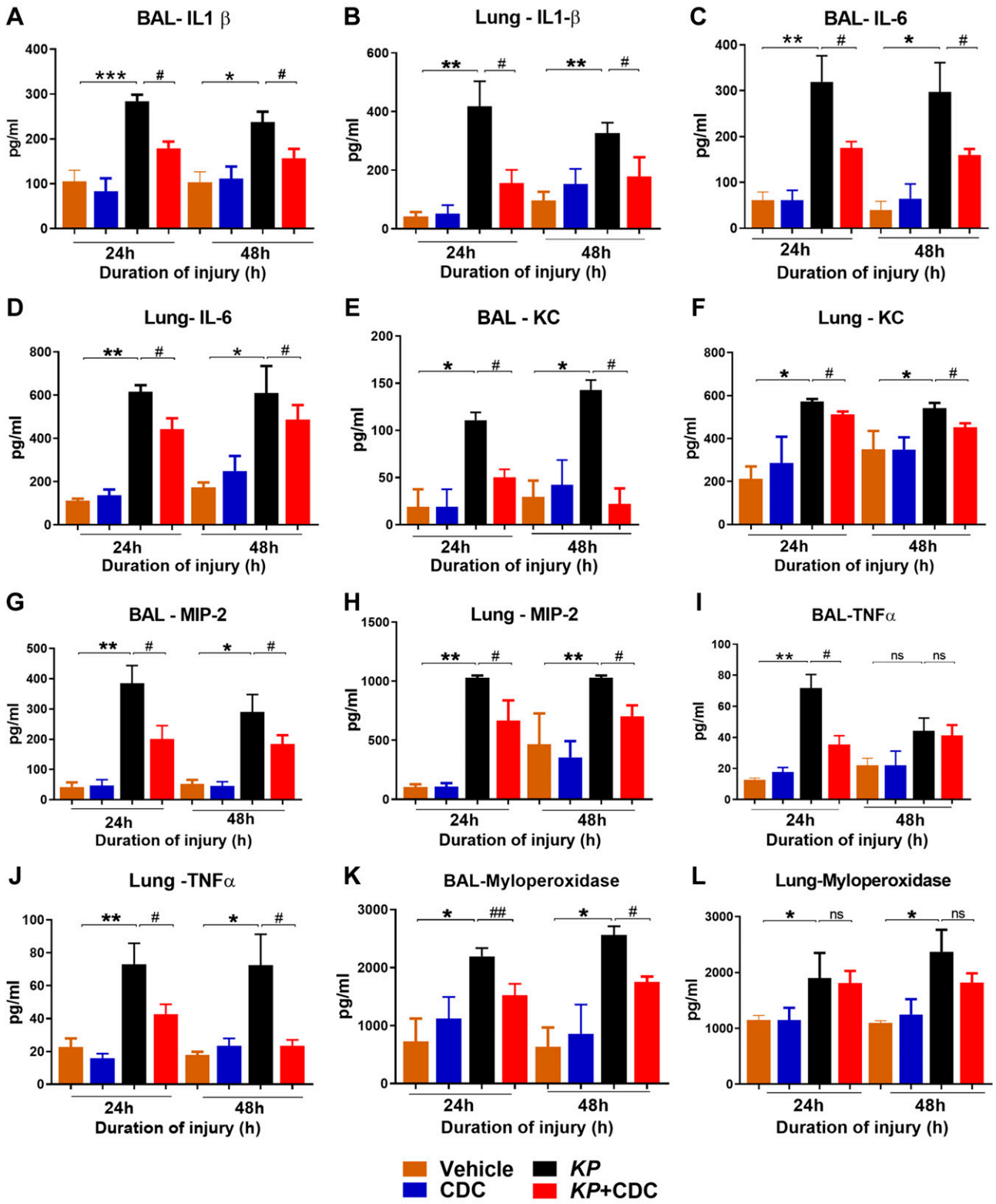

Figure 4. CDC administered mice show reduced inflammation following pneumonia. Cytokine concentrations in the BAL and lungs were determined by ELISA ($n = 16$/group). The levels of IL-1β (*A*, *B*), IL-6 (*C*, *D*), KC (*E*, *F*), MIP-2 (*G*, *H*), TNF-α (*I*, *J*), and MPO (*K*, *L*) were measured. Statistical analysis was performed at each time point. Samples were analyzed using a 2-tailed, unpaired Student's *t* test with Welch's correction. $^{*}P < 0.05$ CDC *vs. KP*; $^{\#}P < 0.05$ *KP vs. KP* + CDC.

CDC, *KP*, and *KP* + CDC mice. The levels of IL-1β, IL-6, and TNF-α were found to be significantly reduced in *KP* mice that received CDC treatment (**Fig. 7*A–C***). The expression of IL-6 and TNF-α were also measured in the lungs at both 24 and 48 h. The expression of IL-6 and TNF-α were significantly lower in *KP* + CDC compared to *KP* mice (Fig. 7*D*, *E*).

Next, the involvement of the inflammasome activity was assessed. Previous work in our laboratory has

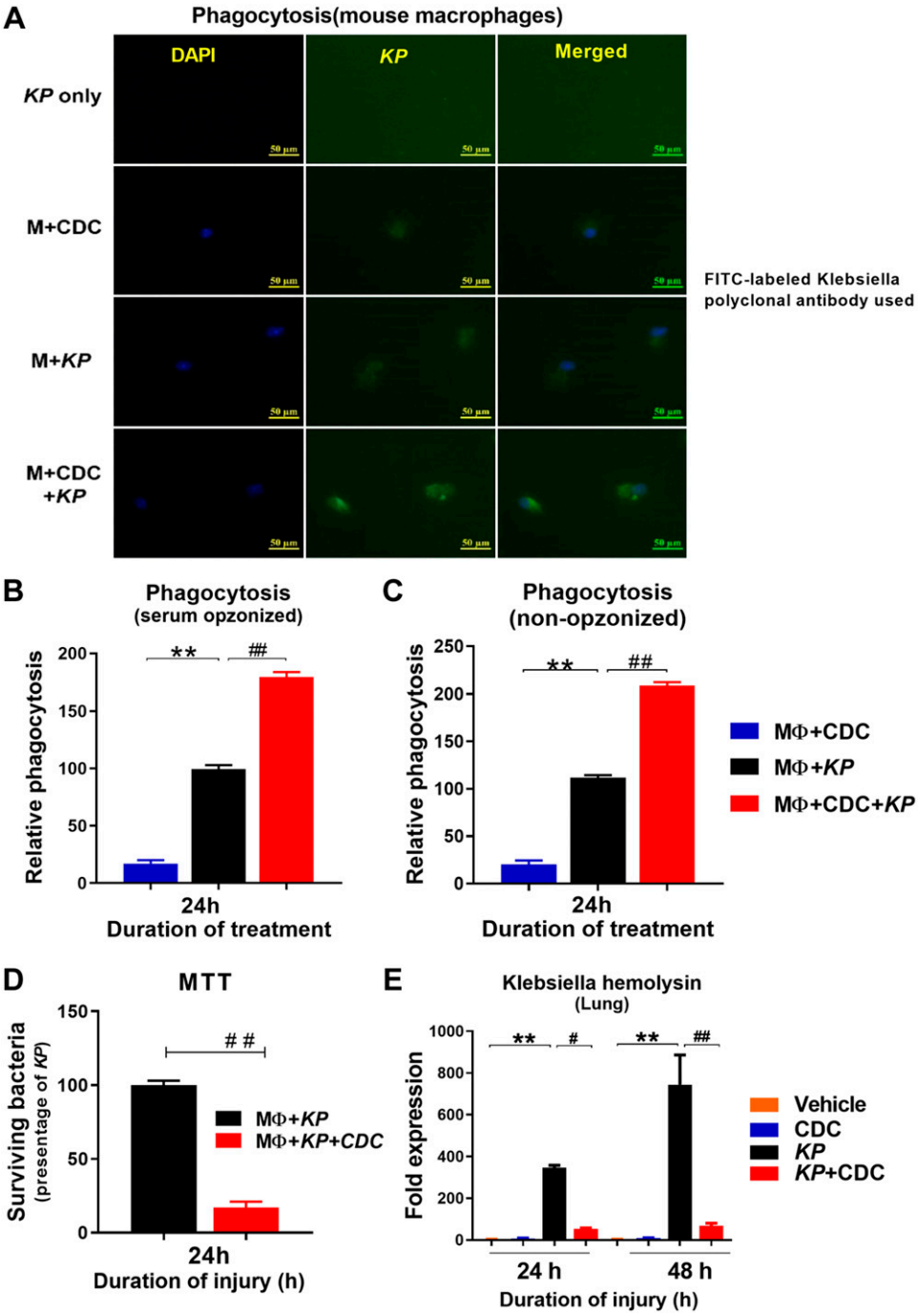

Figure 5. AMs demonstrated increased phagocytosis of *KP* following CDC administration. *A*) Phagocytosis: AM phagocytosis was measured using fluorescence exposure and anti-*KP* antibody. *B*, *C*) *In vitro* serum opsonized (*B*) and nonopsonized (*C*) phagocytosis was also measured (n = 5/group). *D*) MTT assay: Bactericidal activity was performed (n = 5/group). *E*) *Khe* expression: Lung RNA was isolated from the mice in the presence and absence of CDC following pneumonia, and *Khe* expression was measured at 24 and 48 h (n = 5/group). Statistical analysis was performed at each time point. Samples were analyzed using a 2-tailed, unpaired Student's t test with Welch's correction. $^{*}P < 0.05$ CDC *vs.* *KP*; $^{\#}P < 0.05$ *KP vs.* *KP* + CDC.

demonstrated that IL-1β is a critical intermediate involved in the regulation of acute inflammation by type II alveolar epithelial cells (AECs) in other forms of lung injury, such as LC and acid aspiration (5, 37). Here, additional experiments were conducted to determine the lung gene expression of nucleotide-binding domain, leucine-rich–containing family, pyrin domain–containing-3 (NLRP-3) and caspase-1, components of a common inflammasome, as well as IL-1β, an essential product of inflammasome activation, following CDC administration. The expression of IL-1β, NLRP-3, and procaspase-1 was significantly reduced at both 24 and 48 h in *KP* mice that received CDC compared to *KP* alone (Fig. 7*F*–*H*). Additionally, the protein expression of NLRP-3 and caspase-1 was measured by Western blot. The protein levels of both NLRP-3 and caspase-1 were also decreased at both time points in *KP* mice treated with CDC (Fig. 7*I*). These data demonstrate that CDC administration attenuates expression of common inflammatory mediators, including the inflammasome at the level of gene expression following pneumonia.

Viability of AECs is improved in the presence of CDC

The direct impact of *KP* and CDC on A549 human lung epithelial cells viability was also assessed. Cells were

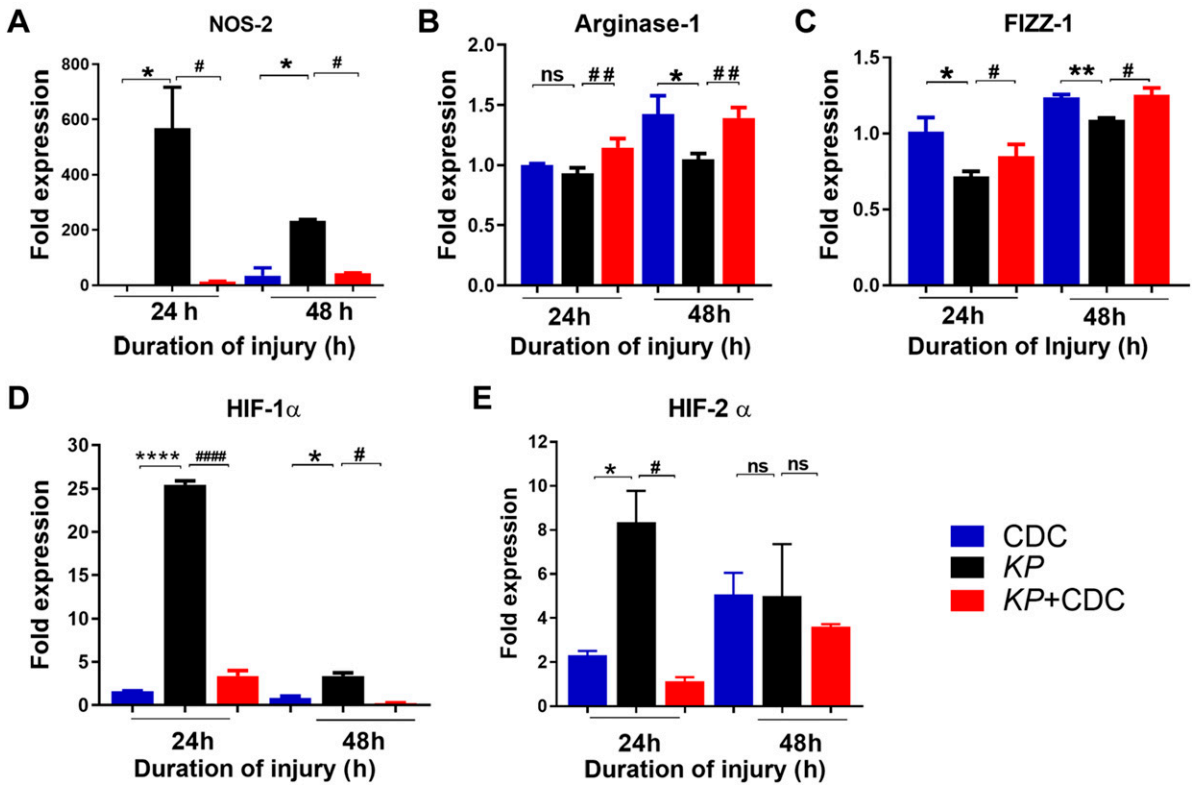

Figure 6. Expression of proinflammatory genes increased following pneumonia. *A–C*) The expressions of lung NOS-2 (*A*), arginase-1 (*B*), and FIZZ-1 (*C*) were measured by real-time PCR following *KP* and CDC administration ($n = 5$/group). Expression of hypoxia-related genes following pneumonia. *D, E*) HIF-1α (*D*) and HIF-2α (*E*) expression was measured ($n = 5$/group). Statistical analysis was performed at each time point. Samples were analyzed using a 2-tailed unpaired Student's *t* test with Welch's correction. $^{*}P < 0.05$ CDC *vs. KP*; $^{\#}P < 0.05$ *KP vs. KP* + CDC.

exposed to CDC, *KP*, and *KP* + CDC. At 24 h, cell viability and morphologic appearance were significantly better preserved in *KP* + CDC mice compared to *KP* alone (Supplemental Fig. S3*A, B*). These data suggest that the CDC can protect the cells from pneumonia infection.

NF-κB activation is reduced following CDC administration

NF-κB (41, 42) is considered the primary proinflammatory mediator of a family of transcription factors involved in many inflammatory disorders and diseases. As we and others have previously shown, HIF-1α acts through a known secondary transcription factor, NF-κB, suggesting an interconnection between NF-κB and HIF-1α signaling (31, 43). Here, total cell extracts from the lungs were harvested at 24 and 48 h and assessed for NF-κBp65 activation by qRT-PCR and Western blot. NF-κBp65 expression was significantly elevated in *KP* mice at 24 and 48 h, but this effect was prevented following CDC administration (**Fig. 8*A***). Moreover, Western blot revealed a significant reduction in the level of NF-κBp65 in *KP* + CDC mice at 24 h, and this reduction occurs as early as within the first 7 h (Fig. 8*B*). Finally, NF-κB activation was evaluated using immunocytochemistry in human lung epithelial cells following *KP*. Cells were harvested at 24 h following inoculation in the absence and presence of CDC and later subjected to immunofluorescence staining with NF-κBp65 (green) and nuclear staining with DAPI. There was intense NF-κBp65 staining in the nucleus of lung epithelial cells following *KP* inoculation. However, CDC administration significantly reduced NF-κB expression compared to cells treated with *KP* alone. There was also a significantly higher degree of cell death following *KP* in the absence of the CDC (Fig. 8*C, D*).

Finally, we measured the expression of phosphorylated NF-κBp65 by Western blot in the lung extracts of *KP* mice in the presence and absence of CDC. Phosphorylated p65 levels were higher at both time points in *KP* mice compared to those that received CDC (Fig. 8*E*). These results suggest that CDC lessens early activation of NF-κB, providing protection on a cellular level.

DISCUSSION

Pneumonia is the leading cause of infectious morbidity and mortality in the United States and is a significant risk factor for ALI and ARDS, both of which are associated with significant mortality (40–60%) (3, 44, 45). In our previous study, we found that plasma concentrations of curcumin and its principal metabolite, tetrahydrocurcumin, were broken down rapidly after 30 min. The rapid clearance of curcumin following systemic CDC administration led us to assess pulmonary administration for subsequent

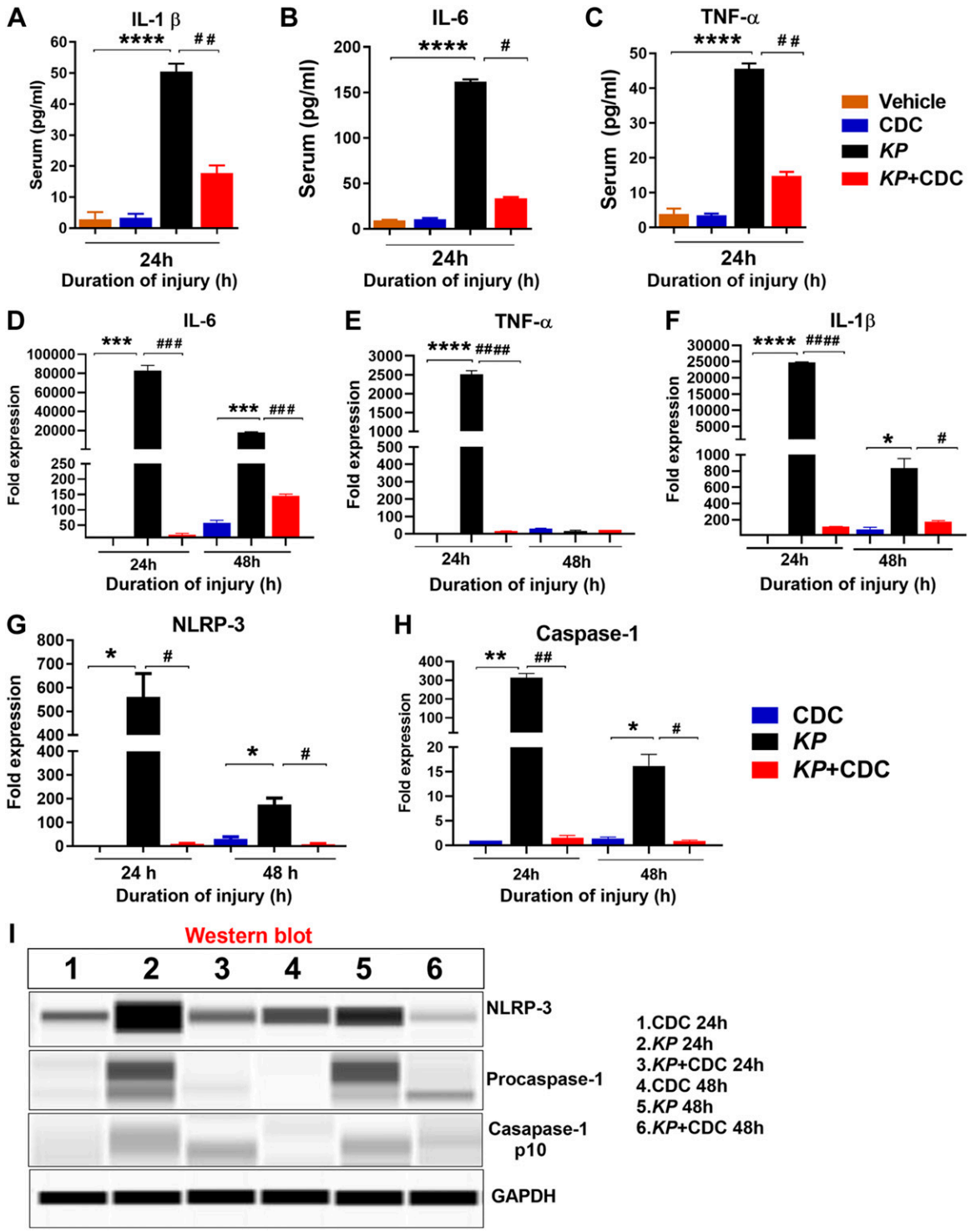

Figure 7. Serum proinflammatory cytokine expression is attenuated by CDC administration. *A–C*) ELISA measured the expression of circulating serum cytokines, including IL-1β (*A*), IL-6 (*B*), and TNF-α (*C*) in *KP* and *KP* + CDC mice ($n = 5$/group). *D–F*) The expression of lung proinflammatory genes IL-6 (*D*), TNF-α (*E*), and IL-1β (*F*) were measured by real-time PCR following in *KP* and *KP* + CDC mice ($n = 5$/group). *G*, *H*) The expression of lung components of inflammasomes, including NLRP-3 (*G*) and procaspase-1 (*H*), was measured by real-time PCR in *KP* and *KP* + CDC mice ($n = 5$/group). *I*) The expression of the whole lung lysate protein NLRP-3 and caspase-1 was measured by Western blot in *KP* and *KP* + CDC mice ($n = 3$/group). Statistical analysis was performed for each time point. Samples were analyzed using a 2-tailed, unpaired Student's *t* test with Welch's correction. $^{*}P < 0.05$ CDC *vs. KP*; $^{\#}P < 0.05$ *KP vs. KP* + CDC.

in vivo studies (24). Previous studies have demonstrated that targeted delivery of CDC to lung cells following exposure to LPS reduces the severity of ALI in mice (16, 46, 47). In the present study, we successfully administered the CDC directly to the lungs *via* deep oral hypopharyngeal injection under isoflurane anesthesia. Here, we sought to

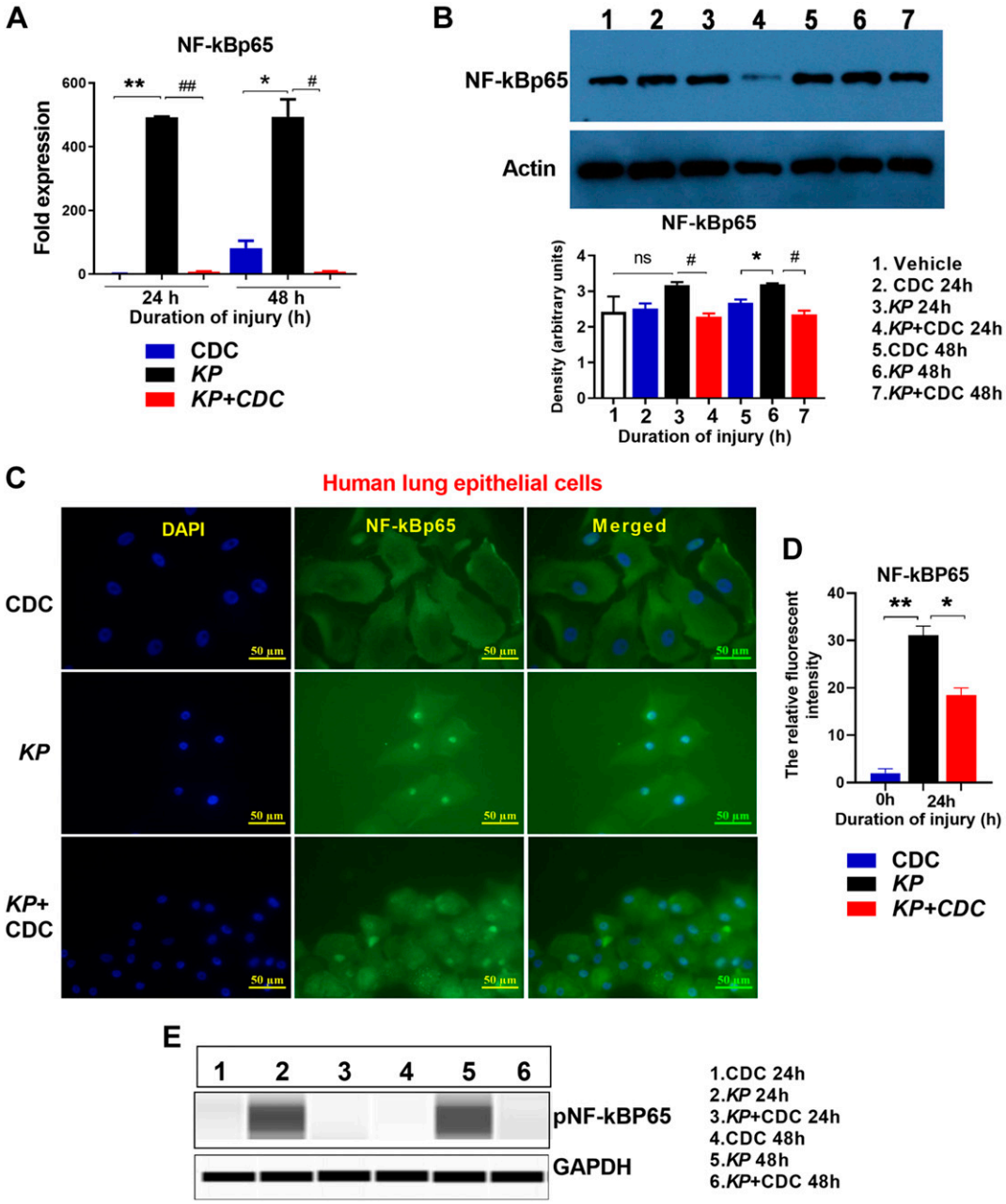

Figure 8. Expression of NF-κB is reduced following CDC administration. *A*, *B*) Mice ($n = 5$/group) were subjected to CDC, *KP*, or *KP* + CDC administration. Lungs were harvested at 24 and 48 h. RNA and protein levels of NF-κB after were measured by qRT-PCR (*A*) and Western blot (*B*), respectively. Immunohistochemistry: NF-κB expression was measured with human lung epithelial cells exposed to *KP* in the presence and absence of CDC ($n = 3$/group). *C*, *D*) The relative fluorescent intensity of NF-κB was analyzed using ImageJ2 software. Mice ($n = 3$/ group) were subjected to CDC, *KP*, or *KP* + CDC. *E*) Lungs were harvested, and phosphorylated NF-κB was measured by Western blot. Samples were analyzed using a 2-tailed, unpaired Student's *t* test with Welch's correction. $^{*}P < 0.05$ CDC *vs. KP*; $^{\#}P < 0.05$ *KP vs. KP* + CDC.

determine the role of CDC in a clinically relevant model of gram-negative bacterial pneumonia in mice to assess the potential to alleviate morbidity and prevent mortality.

In terms of electrical resistance effects on A549 human lung epithelial cells, Peter *et al.* (48) subjected A549 human lung epithelial cells to transepithelial electrical resistance and found that they became leaky at 43.0 ± 1.2 Ωcm^2. Previous studies have also demonstrated the effect of *KP* on A549 human lung epithelial cell remodeling. Ahn *et al.* (49) have shown that *KP*35 infection introduced to BAL cells significantly lessens vital proteins involved in regulating epithelial junctions. This could allow for further accumulation of *KP* and likely result in sepsis. *KP*, then, poses a threat to epithelial cell barrier integrity. In our previous study with Calu-3 cells (24), we observed that epithelial cell monolayer integrity remained intact after transient exposure to CDC at different concentrations. Accordingly, we elected not to measure transepithelial electrical resistance in the present study because it may not be representative of epithelial barrier integrity. Instead, we

sought to determine the effect of CDC on A594 cells exposed to *KP in vitro.*

Previous investigations have revealed the extensive antimicrobial coverage provided by curcumin, both *in vitro* and *in vivo* (16, 24, 46, 47). In the present study, there was total fatality following inoculation with *KP* but significantly improved survival and reduced bacterial burden in both the blood and lungs following early delivery of CDC before 2 h after insult. We further posit that bacteremia was lessened following administration of CDC in part due to the overall decreased severity in lung injury, as evidenced by significant reductions in BAL albumin and degree of histologic injury.

We have previously demonstrated the importance of pro- and anti-inflammatory chemokines and cytokines to the evolution of lung injury (50). Here, we found that treatment with CDC led to broad reductions in the proinflammatory cytokines IL-1β, IL-6, and TNF-α in not just the BAL and lungs but also the serum in the setting of *KP*. Moreover, there was also a concordant decrease in gene expression in the lung following CDC treatment. CDC, therefore, attenuates the inflammatory response at the transcription and protein levels both locally and systemically.

Moreover, the up-regulation of IL-4, arginase-1, and FIZZ-1 indicate M2 AM polarization and an overall improvement in phagocytosis and response to injury (51). Here, we observed the AM phenotype polarization. AM characterization is a vital determinant for the progression of lung injury. The M1 (also termed "classically activated") is characterized by increased production of oxidative burst and simultaneous NO release.

Conversely, the M2 (also termed "alternatively activated") is associated with decreased production of proinflammatory cytokines and up-regulation of the FIZZ-1 pathways. Macrophage polarization dictates the nature, duration, and severity of an inflammatory response (30, 52). Here, we found that M1 activation was significantly higher at 24 h in the *KP* mice when compared to the *KP* + CDC mice (Fig. 2). On the other hand, the M2 was significantly higher in *KP* + CDC compared to *KP* mice (unpublished results). This suggests an avenue of influence by which the CDC formulation decreases inflammation and injury by shifting expression in macrophages away from inflammatory pathways.

The underlying mechanism by which CDC causes down-regulation of injury and inflammation following pneumonia is likely multifactorial and includes modulation of a common inflammasome. The NLRP-3 inflammasome is involved in a range of both sterile and infectious lung disease states including LC and ALI/ARDS. This inflammasome is composed of NLRP-3, the adaptor protein apoptosis-associated speck-like protein containing caspase activation and recruitment domain [CARD (ASC)], and the effector protein caspase-1. Activation involves 2 steps: priming and assembly. Priming is initiated by ligand, such as microbial components or cytokines, binding to IL-1 receptor (IL-1R), TLRs, or TNF receptor (TNF-R). This leads to up-regulation of NF-κB and subsequent expression of inflammasome components. Assembly and activation are then induced by a wide range of damage- or pathogen-associated molecular patterns (DAMPs and PAMPs, respectively) (53, 54).

In the setting of bacterial infection, the NLRP-3 inflammasome has been found to be both helpful and harmful, and in the setting of *KP* it also has a multifaceted role (53). Hua *et al.* (55) studied a serotype of *KP* implicated in pyogenic liver abscess. They identified a virulence factor, K1-CPS, that *in vitro* caused IL-1β up-regulation in macrophages dependent on NLRP-3, ASC, and caspase-1. Moreover, NLRP-3 inflammasome activation by K1-CPS was found to occur through multiple factors including TLR-4, (MAPK, specifically ERK1/2 and p38), PI3K/NF-κB signaling, mitochondrial factors, and in part, through reactive oxygen species (ROS) (55). With a strain of drug-resistant *KP* isolated from patients with bacteremia, Codo *et al.* (56) demonstrated that inflammasome activation was inhibited in macrophages *in vitro*. Specifically, they describe that *KP* induction of IL-10 inhibits inflammasome function, thereby impairing bacterial clearance. Two studies have evaluated the role of the NLRP-3 inflammasome in *KP* murine models of pneumonia (56). Both *in vitro* and *in vivo*, Willingham *et al.* (57) found that NLRP-3 prompts macrophage necrosis as well as expression of the proinflammatory markers high mobility group box 1 and IL-1β. These findings were reversed in not just NLRP-3 but also ASC knockouts. However, although NLRP-3 knockout mice were found to have reductions in inflammation, they also had decreased survival. In another study, Huet *et al.* (58) observed *in vitro* and *in vivo* that glutathione peroxidase 1 knockout mice underwent early NLRP-3 inflammasome activation mediated by H_2O_2. NLRP-3 inflammasome was also associated with improved survival; this effect was reversed not just with antioxidant treatment but also with anakinra, the IL-1R antagonist. NLRP-3, then, is activated by a diversity of factors and appears to play a protective role in *KP* pneumonia.

In the present study, too, *KP* led to up-regulation of NLRP-3 inflammasome activity in a murine model of pneumonia, as indicated by significantly increased expression of NLRP-3, caspase-1, and IL-1β. AMs have been demonstrated to express TLR-2 and TLR-4 and even play a protective role in ALI, including infectious etiologies (54, 55). Here, TLR-2 and TLR-4, which are also involved in inflammasome priming, were found to be elevated in the lungs after *KP* without any deleterious effect on injury or survival. RNA and protein expression of NF-κB were also significantly elevated following *KP*. Bacterial burden and mortality were significantly increased due to *KP*. These findings, however, were reversed with CDC administration. Contrary to other studies in which NLRP-3 was found to be protective, here down-regulation by CDC was associated with decreased bacterial dissemination, inflammation, and mortality. The mechanism of NLRP-3 inflammasome down-regulation by CDC is likely multifactorial and includes modulation of priming *via* TLRs and NF-κB as well as possibly ROS, MAPK signaling, or HIF-related pathways through hypoxic AECs, as we have previously described (37).

We have recently found that FER, a tyrosine-protein kinase gene, is involved in the recruitment and activation of inflammatory monocytes and macrophages as well as in modifications of known signaling transduction pathways that enhance bacterial clearance and improve survival (26, 27). Here, we found that FER expression was significantly higher following CDC

administration (Supplemental Fig. S2). Bacterial lung infection is characterized by excessive capillary leakage, activation of transcription factors, expression of proinflammatory mediators, and accumulation of neutrophils in the alveolar spaces with diffuse damage to the alveolar epithelial and endothelial cells (59, 60). Our research has previously demonstrated that HIF-1α plays a critical role in the regulation of inflammation following lung injury, specifically, through type II AECs (31, 37). Here, the expression of both HIF-1α and HIF-2α were decreased following treatment with CDC.

Furthermore, HIF and NF-κB are known to regulate the response to hypoxia and inflammation in tandem (61). Xu *et al.* (47) recently reported that curcumin reduces macrophage activation and lung inflammation induced by influenza infection through inhibition of the NF-κB signaling pathway. Here, we report that CDC administration significantly reduced expression of NF-κB at both the transcript and protein levels. CDC, therefore, likely further attenuates inflammation following bacterial pneumonia *via* modulation of the interconnected HIF and NF-κB proinflammatory pathways.

To our knowledge, this is the first study that conclusively demonstrates the benefits of a specific curcumin formulation on injury, inflammation, and survival in a lethal gram-negative model of pneumonia. Early direct delivery of the CDC likely prevents injury and inflammation through preferential polarization of M2s and modulation of HIF-related pathways, including NF-κB. Of note, studies in humans have found that curcumin is generally well tolerated without adverse effects, except for diarrhea at extremely high oral doses (20, 24). Direct delivery of CDC to the lungs is a safe and effective therapy in a murine model of gram-negative pneumonia. These promising results support further evaluation of the role of CDC in human pneumonia and other inflammatory lung injuries such as ARDS. FJ

ACKNOWLEDGMENTS

The authors gratefully acknowledge the support of U.S. National Institutes of Health, National Institute of General Medical Sciences Grant R01 GM111305-01 (to K.R.). The authors declare no conflicts of interest.

AUTHOR CONTRIBUTIONS

J. Parkkinen, K. Raghavendran, and M. V. Suresh conceived and designed the study; B. Zhang, S. Swamy, S. Balijepalli, S. Panicker, J. Mooliyil, and M. V. Suresh performed research; K. Raghavendran and M. V. Suresh performed analysis and interpretation; and M. A. Sherman, J. Parkkinen, K. Raghavendran, and M. V. Suresh drafted the manuscript for important intellectual content.

REFERENCES

1. Miller, P. R., Croce, M. A., Bee, T. K., Qaisi, W. G., Smith, C. P., Collins, G. L., and Fabian, T. C. (2001) ARDS after pulmonary contusion: accurate measurement of contusion volume identifies high-risk patients. *J. Trauma* **51**, 223–228; discussion 229–230
2. Arroliga, A. C., Ghamra, Z. W., Perez Trepichio, A., Perez Trepichio, P., Komara, J. J., Jr., Smith, A., and Wiedemann, H. P. (2002) Incidence of ARDS in an adult population of northeast Ohio. *Chest* **121**, 1972–1976
3. Cochi, S. E., Kempker, J. A., Annangi, S., Kramer, M. R., and Martin, G. S. (2016) Mortality trends of acute respiratory distress syndrome in the United States from 1999 to 2013. *Ann. Am. Thorac. Soc.* **13**, 1742–1751
4. Steinhauser, M. L., Hogaboam, C. M., Kunkel, S. L., Lukacs, N. W., Strieter, R. M., and Standiford, T. J. (1999) IL-10 is a major mediator of sepsis-induced impairment in lung antibacterial host defense. *J. Immunol.* **162**, 392–399
5. Suresh, M. V., Balijepalli, S., Zhang, B., Singh, V. V., Swamy, S., Panicker, S., Dolgachev, V. A., Subramanian, C., Ramakrishnan, S. K., Thomas, B., Rao, T. C., Delano, M. J., Machado-Aranda, D., Shah, Y. M., and Raghavendran, K. (2018) Hypoxia-inducible factor (HIF)-1α promotes inflammation and injury following aspiration-induced lung injury in mice. [E-pub ahead of print] *Shock*
6. Davidson, B. A., Knight, P. R., Helinski, J. D., Nader, N. D., Shanley, T. P., and Johnson, K. J. (1999) The role of tumor necrosis factor-alpha in the pathogenesis of aspiration pneumonitis in rats. *Anesthesiology* **91**, 486–499
7. Hoth, J. J., Hudson, W. P., Brownlee, N. A., Yoza, B. K., Hiltbold, E. M., Meredith, J. W., and McCall, C. E. (2007) Toll-like receptor 2 participates in the response to lung injury in a murine model of pulmonary contusion. *Shock* **28**, 447–452
8. Bauer, T. T., Ferrer, R., Angrill, J., Schultze-Werninghaus, G., and Torres, A. (2000) Ventilator-associated pneumonia: incidence, risk factors, and microbiology. *Semin. Respir. Infect.* **15**, 272–279
9. Kochanek, K. D., Murphy, S. L., Xu, J., and Arias, E. (2014) Mortality in the United States, 2013. *NCHS Data Brief* **178**, 1–8
10. Iregui, M., Ward, S., Sherman, G., Fraser, V. J., and Kollef, M. H. (2002) Clinical importance of delays in the initiation of appropriate antibiotic treatment for ventilator-associated pneumonia. *Chest* **122**, 262–268
11. Seligman, R., Papassotiriou, J., Morgenthaler, N. G., Meisner, M., and Teixeira, P. J. (2008) Copeptin, a novel prognostic biomarker in ventilator-associated pneumonia. *Crit. Care* **12**, R11
12. Takala, A., Nupponen, I., Kylänpää-Bäck, M. L., and Repo, H. (2002) Markers of inflammation in sepsis. *Ann. Med.* **34**, 614–623
13. Ayodele, O. E., Okpechi, I. G., and Swanepoel, C. R. (2010) Predictors of poor renal outcome in patients with biopsy-proven lupus nephritis. *Nephrology (Carlton)* **15**, 482–490
14. Bauer, T. T., Ewig, S., Rodloff, A. C., and Müller, E. E. (2006) Acute respiratory distress syndrome and pneumonia: a comprehensive review of clinical data. *Clin. Infect. Dis.* **43**, 748–756
15. Aggarwal, B. B., Yuan, W., Li, S., and Gupta, S. C. (2013) Curcumin-free turmeric exhibits anti-inflammatory and anticancer activities: identification of novel components of turmeric. *Mol. Nutr. Food Res.* **57**, 1529–1542
16. Wang, X., Hang, Y., Liu, J., Hou, Y., Wang, N., and Wang, M. (2017) Anticancer effect of curcumin inhibits cell growth through miR-21/PTEN/Akt pathway in breast cancer cell. *Oncol. Lett.* **13**, 4825–4831
17. Reddy, P. H., Manczak, M., Yin, X., Grady, M. C., Mitchell, A., Tonk, S., Kuruva, C. S., Bhatti, J. S., Kandimalla, R., Vijayan, M., Kumar, S., Wang, R., Pradeepkiran, J. A., Ogunmokun, G., Thamarai, K., Quesada, K., Boles, A., and Reddy, A. P. (2018) Protective effects of Indian spice curcumin against amyloid-β in Alzheimer's disease. *J. Alzheimers Dis.* **61**, 843–866
18. Sun, Y., Liu, W., Zhang, H., Li, H., Liu, J., Zhang, F., Jiang, T., and Jiang, S. (2017) Curcumin prevents osteoarthritis by inhibiting the activation of inflammasome NLRP3. *J. Interferon Cytokine Res.* **37**, 449–455
19. Sharma, N., and Nehru, B. (2018) Curcumin affords neuroprotection and inhibits α-synuclein aggregation in lipopolysaccharide-induced Parkinson's disease model. *Inflammopharmacology* **26**, 349–360
20. Qin, S., Huang, L., Gong, J., Shen, S., Huang, J., Ren, H., and Hu, H. (2017) Efficacy and safety of turmeric and curcumin in lowering blood lipid levels in patients with cardiovascular risk factors: a meta-analysis of randomized controlled trials. *Nutr. J.* **16**, 68
21. Fadus, M. C., Lau, C., Bikhchandani, J., and Lynch, H. T. (2016) Curcumin: an age-old anti-inflammatory and anti-neoplastic agent. *J. Tradit. Complement. Med.* **7**, 339–346
22. Cooney, J. M., Barnett, M. P., Dommels, Y. E., Brewster, D., Butts, C. A., McNabb, W. C., Laing, W. A., and Roy, N. C. (2016) A combined omics approach to evaluate the effects of dietary curcumin on colon inflammation in the Mdr1a(-/-) mouse model of inflammatory bowel disease. *J. Nutr. Biochem.* **27**, 181–192
23. Tønnesen, H. H., Másson, M., and Loftsson, T. (2002) Studies of curcumin and curcuminoids. XXVII. Cyclodextrin complexation: solubility, chemical and photochemical stability. *Int. J. Pharm.* **244**, 127–135
24. Suresh, M. V., Wagner, M. C., Rosania, G. R., Stringer, K. A., Min, K. A., Risler, L., Shen, D. D., Georges, G. E., Reddy, A. T., Parkkinen, J., and

Reddy, R. C. (2012) Pulmonary administration of a water-soluble curcumin complex reduces severity of acute lung injury. *Am. J. Respir. Cell Mol. Biol.* **47**, 280–287
25. Saidi, S. A., Meurisse, N., Jochmans, I., Heedfeld, V., Wylin, T., Parkkinen, J., Pirenne, J., Monbaliu, D., El Feki, A., and van Pelt, J. (2018) Hepatocellular uptake of cyclodextrin-complexed curcumin during liver preservation: a feasibility study. *Biopharm. Drug Dispos.* **39**, 18–29
26. Dolgachev, V., Panicker, S., Balijepalli, S., McCandless, L. K., Yin, Y., Swamy, S., Suresh, M. V., Delano, M. J., Hemmila, M. R., Raghavendran, K., and Machado-Aranda, D. (2018) Electroporation-mediated delivery of FER gene enhances innate immune response and improves survival in a murine model of pneumonia. *Gene Ther.* **25**, 359–375
27. Dolgachev, V. A., Goldberg, R., Suresh, M. V., Thomas, B., Talarico, N., Hemmila, M. R., Raghavendran, K., and Machado-Aranda, D. (2016) Electroporation-mediated delivery of the FER gene in the resolution of trauma-related fatal pneumonia. *Gene Ther.* **23**, 785–796
28. Dolgachev, V. A., Yu, B., Reinke, J. M., Raghavendran, K., and Hemmila, M. R. (2012) Host susceptibility to gram-negative pneumonia after lung contusion. *J. Trauma Acute Care Surg.* **72**, 614–622; discussion 622–623
29. Obi, A. T., Andraska, E., Kanthi, Y., Luke, C. E., Elfline, M., Madathilparambil, S., Siahaan, T. J., Jaffer, F. A., Wakefield, T. W., Raghavendran, K., and Henke, P. K. (2016) Gram-negative pneumonia alters large-vein cell-adhesion molecule profile and potentiates experimental stasis venous thrombosis. *J. Vasc. Res.* **53**, 186–195
30. Suresh, M. V., Thomas, B., Machado-Aranda, D., Dolgachev, V. A., Kumar Ramakrishnan, S., Talarico, N., Cavassani, K., Sherman, M. A., Hemmila, M. R., Kunkel, S. L., Walter, N. G., Hogaboam, C. M., and Raghavendran, K. (2016) Double-stranded RNA interacts with toll-like receptor 3 in driving the acute inflammatory response following lung contusion. *Crit. Care Med.* **44**, e1054–e1066
31. Suresh, M. V., Ramakrishnan, S. K., Thomas, B., Machado-Aranda, D., Bi, Y., Talarico, N., Anderson, E., Yatrik, S. M., and Raghavendran, K. (2014) Activation of hypoxia-inducible factor-1α in type 2 alveolar epithelial cell is a major driver of acute inflammation following lung contusion. *Crit. Care Med.* **42**, e642–e653
32. Suresh, M. V., Yu, B., Lakshminrusimha, S., Machado-Aranda, D., Talarico, N., Zeng, L., Davidson, B. A., Pennathur, S., and Raghavendran, K. (2013) The protective role of MnTBAP in oxidant-mediated injury and inflammation in a rat model of lung contusion. *Surgery* **154**, 980–990
33. Suresh, M. V., Yu, B., Machado-Aranda, D., Bender, M. D., Ochoa-Frongia, L., Helinski, J. D., Davidson, B. A., Knight, P. R., Hogaboam, C. M., Moore, B. B., and Raghavendran, K. (2012) Role of macrophage chemoattractant protein-1 in acute inflammation after lung contusion. *Am. J. Respir. Cell Mol. Biol.* **46**, 797–806
34. Serezani, C. H., Aronoff, D. M., Jancar, S., Mancuso, P., and Peters-Golden, M. (2005) Leukotrienes enhance the bactericidal activity of alveolar macrophages against Klebsiella pneumoniae through the activation of NADPH oxidase. *Blood* **106**, 1067–1075
35. Beekman, C., Janson, A. A., Baghat, A., van Deutekom, J. C., and Datson, N. A. (2018) Use of capillary Western immunoassay (Wes) for quantification of dystrophin levels in skeletal muscle of healthy controls and individuals with Becker and Duchenne muscular dystrophy. *PLoS One* **13**, e0195850
36. Zheng, C. Y., Petralia, R. S., Wang, Y. X., and Kachar, B. (2011) Fluorescence recovery after photobleaching (FRAP) of fluorescence tagged proteins in dendritic spines of cultured hippocampal neurons. *J. Vis. Exp.* **50**, 2568
37. Sherman, M. A., Suresh, M. V., Dolgachev, V. A., McCandless, L. K., Xue, X., Ziru, L., Machado-Aranda, D., Shah, Y. M., and Raghavendran, K. (2018) Molecular characterization of hypoxic alveolar epithelial cells after lung contusion indicates an important role for HIF-1α. *Ann. Surg.* **267**, 382–391
38. Ward, P. A., and Lentsch, A. B. (1999) The acute inflammatory response and its regulation. *Arch. Surg.* **134**, 666–669
39. Karo-Atar, D., Bordowitz, A., Wand, O., Pasmanik-Chor, M., Fernandez, I. E., Itan, M., Frenkel, R., Herbert, D. R., Finkelman, F. D., Eickelberg, O., and Munitz, A. (2016) A protective role for IL-13 receptor α 1 in bleomycin-induced pulmonary injury and repair. *Mucosal Immunol.* **9**, 240–253
40. Standiford, T. J., Kunkel, S. L., Greenberger, M. J., Laichalk, L. L., and Strieter, R. M. (1996) Expression and regulation of chemokines in bacterial pneumonia. *J. Leukoc. Biol.* **59**, 24–28
41. D'Ignazio, L., and Rocha, S. (2016) Hypoxia induced NF-κB. *Cells* **5**, E10
42. Jung, Y. J., Isaacs, J. S., Lee, S., Trepel, J., and Neckers, L. (2003) IL-1beta-mediated up-regulation of HIF-1alpha via an NFkappaB/COX-2 pathway identifies HIF-1 as a critical link between inflammation and oncogenesis. *FASEB J.* **17**, 2115–2117
43. D'Ignazio, L., Bandarra, D., and Rocha, S. (2016) NF-κB and HIF crosstalk in immune responses. *FEBS J.* **283**, 413–424
44. Chen, W., Chen, Y. Y., Tsai, C. F., Chen, S. C., Lin, M. S., Ware, L. B., and Chen, C. M. (2015) Incidence and outcomes of acute respiratory distress syndrome: a Nationwide registry-based study in Taiwan, 1997 to 2011. *Medicine (Baltimore)* **94**, e1849
45. Riviello, E. D., Kiviri, W., Twagirumugabe, T., Mueller, A., Banner-Goodspeed, V. M., Officer, L., Novack, V., Mutumwinka, M., Talmor, D. S., and Fowler, R. A. (2016) Hospital incidence and outcomes of the acute respiratory distress syndrome using the kigali modification of the Berlin definition. *Am. J. Respir. Crit. Care Med.* **193**, 52–59
46. Jin, C. Y., Lee, J. D., Park, C., Choi, Y. H., and Kim, G. Y. (2007) Curcumin attenuates the release of pro-inflammatory cytokines in lipopolysaccharide-stimulated BV2 microglia. *Acta Pharmacol. Sin.* **28**, 1645–1651
47. Xu, Y., and Liu, L. (2017) Curcumin alleviates macrophage activation and lung inflammation induced by influenza virus infection through inhibiting the NF-κB signaling pathway. *Influenza Other Respir. Viruses* **11**, 457–463
48. Peter, Y., Comellas, A., Levantini, E., Ingenito, E. P., and Shapiro, S. D. (2009) Epidermal growth factor receptor and claudin-2 participate in A549 permeability and remodeling: implications for non-small cell lung cancer tumor colonization. *Mol. Carcinog.* **48**, 488–497
49. Ahn, D., Wickersham, M., Riquelme, S., and Prince, A. (2019) The effects of IFN-λ on epithelial barrier function contribute to Klebsiella pneumoniae ST258 pneumonia. *Am. J. Respir. Cell Mol. Biol.* **60**, 158–166
50. Raghavendran, K., Davidson, B. A., Woytash, J. A., Helinski, J. D., Marschke, C. J., Manderscheid, P. A., Notter, R. H., and Knight, P. R. (2005) The evolution of isolated bilateral lung contusion from blunt chest trauma in rats: cellular and cytokine responses. *Shock* **24**, 132–138
51. Ishii, M., Wen, H., Corsa, C. A., Liu, T., Coelho, A. L., Allen, R. M., Carson IV, W. F., Cavassani, K. A., Li, X., Lukacs, N. W., Hogaboam, C. M., Dou, Y., and Kunkel, S. L. (2009) Epigenetic regulation of the alternatively activated macrophage phenotype. *Blood* **114**, 3244–3254
52. Machado-Aranda, D. A., Suresh, M. V., Yu, B., and Raghavendran, K. (2012) Electroporation-mediated *in vivo* gene delivery of the Na+/K+-ATPase pump reduced lung injury in a mouse model of lung contusion. *J. Trauma Acute Care Surg.* **72**, 32–39; discussion 39–40
53. Kim, J. J., and Jo, E. K. (2013) NLRP3 inflammasome and host protection against bacterial infection. *J. Korean Med. Sci.* **28**, 1415–1423
54. He, Y., Hara, H., and Núñez, G. (2016) Mechanism and regulation of NLRP3 inflammasome activation. *Trends Biochem. Sci.* **41**, 1012–1021
55. Hua, K. F., Yang, F. L., Chiu, H. W., Chou, J. C., Dong, W. C., Lin, C. N., Lin, C. Y., Wang, J. T., Li, L. H., Chiu, H. W., Chiu, Y. C., and Wu, S. H. (2015) Capsular polysaccharide is involved in NLRP3 inflammasome activation by Klebsiella pneumoniae serotype K1. *Infect. Immun.* **83**, 3396–3409
56. Codo, A. C., Saraiva, A. C., Dos Santos, L. L., Visconde, M. F., Gales, A. C., Zamboni, D. S., and Medeiros, A. I. (2018) Inhibition of inflammasome activation by a clinical strain of Klebsiella pneumoniae impairs efferocytosis and leads to bacterial dissemination. *Cell Death Dis.* **9**, 1182
57. Willingham, S. B., Allen, I. C., Bergstralh, D. T., Brickey, W. J., Huang, M. T., Taxman, D. J., Duncan, J. A., and Ting, J. P. (2009) NLRP3 (NALP3, Cryopyrin) facilitates *in vivo* caspase-1 activation, necrosis, and HMGB1 release via inflammasome-dependent and -independent pathways. *J. Immunol.* **183**, 2008–2015
58. Huet, O., Pickering, R. J., Tikellis, C., Latouche, C., Long, F., Kingwell, B., Dickinson, B., Chang, C. J., Masters, S., Mackay, F., Cooper, M. E., and de Haan, J. B. (2017) Protective effect of inflammasome activation by hydrogen peroxide in a mouse model of septic shock. *Crit. Care Med.* **45**, e184–e194
59. Strieter, R. M., and Kunkel, S. L. (1994) Acute lung injury: the role of cytokines in the elicitation of neutrophils. *J. Investig. Med.* **42**, 640–651
60. Cai, S., Batra, S., Lira, S. A., Kolls, J. K., and Jeyaseelan, S. (2010) CXCL1 regulates pulmonary host defense to Klebsiella infection via CXCL2, CXCL5, NF-kappaB, and MAPKs. *J. Immunol.* **185**, 6214–6225
61. Taylor, M., Qu, A., Anderson, E. R., Matsubara, T., Martin, A., Gonzalez, F. J., and Shah, Y. M. (2011) Hypoxia-inducible factor-2α mediates the adaptive increase of intestinal ferroportin during iron deficiency in mice. *Gastroenterology* **140**, 2044–2055

Received for publication April 23, 2019.
Accepted for publication August 19, 2019.